

ARTICLE OPEN



Interannual variation in the East Asian summer monsoon-tropical Atlantic SST relationship modulated by the Interdecadal Pacific Oscillation

Hao Wang ¹, Ziguang Li ^{1,2}✉, Jianping Li ^{1,2}, Xiaopei Lin ^{1,2}, Xiao-Tong Zheng ^{1,2}, Lei Fan ¹ and Yu Zhang ^{1,2}

Tropical Atlantic (TA) SST variability can impact the East Asian summer monsoon (EASM). Here, we find that the interannual EASM-TA relationship exhibits an evident interdecadal variation modulated by the Interdecadal Pacific Oscillation (IPO). The EASM-TA interannual relationship is strong during the positive phase of the IPO (pIPO) but weak during the negative phase of the IPO (nIPO). The pIPO (nIPO)-related warm (cold) SST anomalies in the central tropical Pacific (CTP) intensify (weaken) the convection over the CTP. Therefore, a Matsuno–Gill response of the TA-induced CTP SST change is strong (weak) during the pIPO (nIPO) period. The strong Matsuno–Gill response excites an anomalous anticyclone over the western North Pacific (WNPAC), leading to a significantly positive EASM-TA relationship. However, the WNPAC is absent in the nIPO periods due to the weak Matsuno–Gill response, suggesting an insignificant EASM-TA relationship. Understanding the IPO-modulated EASM-TA relationship helps better forecast EASM variability.

npj Climate and Atmospheric Science (2023)6:169; <https://doi.org/10.1038/s41612-023-00497-x>

INTRODUCTION

The East Asian summer monsoon (EASM) is one of the most prominent climatic features in East Asia^{1,2}, transporting large amounts of heat and vapor to this most populated region from the tropics³. Interannual fluctuation in the EASM leads to flood or drought, exerting tremendous socio-economic influence on the surrounding countries^{4–6}. Previous studies have identified many climate variabilities that can affect the EASM on interannual timescales, such as the El Niño-Oscillation (ENSO)^{1,7–11}, Indian Ocean Basin Mode^{12–15}, Arctic Oscillation¹⁶, and North Atlantic Oscillation^{17–19}. Sea surface temperature (SST) variability in the tropical Atlantic (TA)—as a recently identified factor—provides an important insight into understanding the dynamics of the EASM and improving its prediction^{20–22}.

There are two dominant modes of SST variability in the TA on interannual timescales—the Atlantic zonal mode (also referred to as the Atlantic Niño)²³ and the Atlantic meridional mode^{22,24–26}. The center of action of the Atlantic Niño is located in the southeastern TA, while the Atlantic meridional mode is mainly situated in the northern TA. The two modes have different climatic influences; that is, the Atlantic meridional mode has a more obvious impact on low-level anomalous anticyclones over the western North Pacific (WNPAC) and can better represent the influences of TA on climate variability in East Asia than the Atlantic zonal mode^{22,27,28}. It was found that the Atlantic meridional mode-associated warm SST anomalies in the northern TA can change the Walker circulation with descending motion over the central tropical Pacific (CTP) and ascending motion over the TA on both interannual and decadal timescales^{20,22,29–35}. The anomalous descending motion over the CTP leads to a diabatic cooling effect over the CTP, which in turn excites the WNPAC via the Matsuno–Gill response and thus further intensifies the strength of the EASM^{1,20,22,31,36}. The opposite processes operate for the cold

TA SST anomalies, which can excite low-level anomalous cyclones over the WNPAC to weaken the strength of the EASM.

However, the relationship between the EASM and its interannual influencing factor is always unstable, meaning that there may be a dominant climate variability longer than interannual timescales that modulate the relationship^{7,37–40}. The Interdecadal Pacific Oscillation (IPO) is the leading mode of SST variability in the entire Pacific on interdecadal timescales, controlling the mean state of the whole Pacific^{41–44}. The IPO is considered an interdecadal controller of the unstable EASM-ENSO relationship through modulating the mean state in the subtropical western Pacific³⁸. Specifically, during the positive phase of the IPO (pIPO), the warm SST anomalies in the Eastern China Sea led to a weakened subtropical high and increased precipitation over the western North Pacific (WNP)³⁸. The ENSO-induced atmospheric Kelvin wave favors a stronger response over the WNP because of the weakened subtropical high, leading to a strong EASM-ENSO relationship³⁸. On the contrary, the negative phase of the IPO (nIPO) favors a weak EASM-ENSO relationship via the opposite processes. Since the SST in the TA is the recently identified factor for the EASM on interannual timescales, is their relationship unstable on interdecadal timescales? If any, the role of the low-frequency quantity (such as the IPO and the Atlantic Multidecadal Oscillation (AMO)^{45,46} in modulating this relationship needs to be investigated.

RESULTS

Interdecadal variation in the EASM-TA relationship

To examine the relationship between the EASM and SST anomalies over the TA, we calculate the correlation map between SST anomalies and the EASM index. As shown in Fig. 1a, there is a large area in the TA where SST is significantly correlated with the EASM, showing a positive EASM-TA relationship. The significantly

¹Physical Oceanography Laboratory/Frontiers Science Center for Deep Ocean Multispheres and Earth System/Sanya Oceanographic Institution, Ocean University of China, Qingdao, China. ²Laoshan Laboratory, Qingdao, China. ✉email: ziguangli@ouc.edu.cn

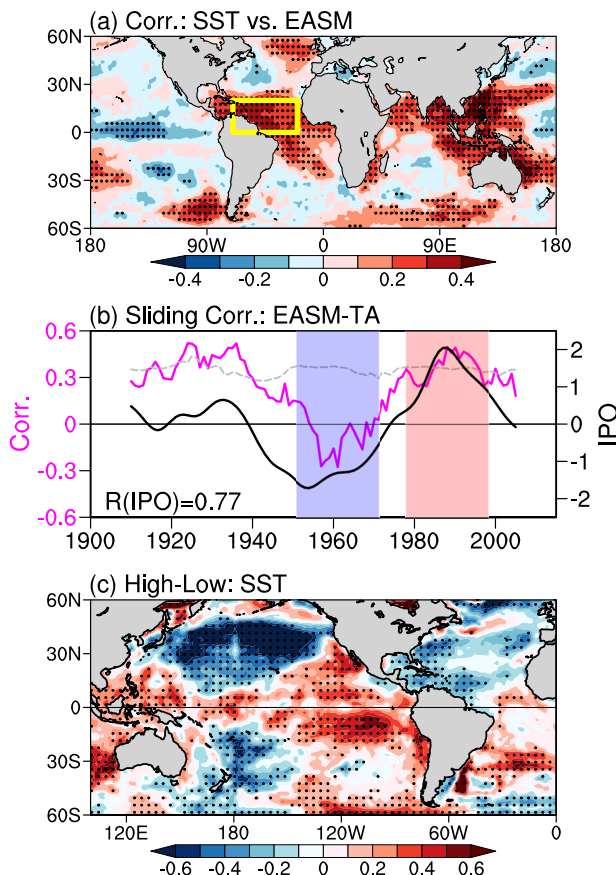


Fig. 1 The interdecadal variation in the EASM-TA relationship and its linkage with the IPO. **a**, Correlation map between JJA sea surface temperature and the EASM index. **b**, The 21-year sliding correlation between the EASM index and the TA sea surface temperature index (solid magenta line), which is superimposed by the IPO index (solid black line). **c**, Composite difference of SST anomalies ($^{\circ}\text{C}$) between the highly correlated and insignificantly correlated periods of the EASM and TA SST. The yellow rectangle box in **a** denotes the domain of TA. The dotted area in **a** indicates the correlation coefficient, which is significant at the 95% confidence level using the student's *t*-test. The gray dashed line in **b** indicates the running correlation coefficient, which is significant at the 95% confidence level using Student's *t*-test. The blue (red) rectangle box presents the period of the negative (positive) phase of the IPO from 1951 to 1971 (1978–1998). The dotted area in **(c)** indicates the SST difference, which is significant at the 95% confidence level using Student's *t*-test.

correlated area is mainly located in the northern tropical Atlantic, which resembles the Atlantic meridional mode (the correlation coefficient between the TA and Atlantic meridional mode is 0.99). However, the Atlantic zonal mode mainly highlights SST variability in the southeastern tropical Atlantic²², which is insignificantly correlated with the EASM (Fig. 1a). Therefore, we focus on the northern TA and define TA SST index as the June–July–August (JJA) SST anomalies averaged over 70°W – 20°W , 0° – 20°N (yellow box in Fig. 1a). Then, we perform the sliding correlation analysis with a 21-year window to show the interdecadal variation in the EASM-TA relationship (Fig. 1b, solid magenta line). The correlation coefficients show obvious interdecadal variation, ranging from the lowest (-0.27) to highest (0.53) value. Hence, the EASM-TA relationship is not stationary but with substantial temporal details compared to a single correlation coefficient derived from the long-term perspective. We have also used another dataset to examine if this relationship exists (Supplementary Fig. 1). It is clear

that the results under different datasets are similar, highlighting the reliability of the results.

What causes the interdecadal variation in the EASM-TA relationship? The changing EASM-TA relationship must be modulated by a certain climate variability that is longer than interannual timescales. In order to find the interdecadal modulator of the EASM-TA relationship, two periods are selected based on the correlation coefficient between the EASM and TA. The period of 1978–1998 represents the period when the EASM is highly correlated with TA SST (the red box in Fig. 1b), while the period of 1951–1971 represents the period when the EASM is insignificantly correlated with TA SST (the blue box in Fig. 1b). The composite difference of SST anomalies between these two periods represents a pattern that resembles the IPO in the Pacific (Fig. 1c). Besides, the temporal evolution of the EASM-TA relationship is also similar to that of the IPO (solid black line in Fig. 1b), with a correlation coefficient of 0.79, above the 95% confidence level. However, a large area in the northern Atlantic exhibits insignificant differences between the two periods. Besides, the time series of the EASM-TA relationship is insignificantly correlated with the AMO, with a correlation coefficient of -0.04 , far below the 80% confidence level (Supplementary Fig. 2). These results indicate that the IPO is likely to be the interdecadal modulator of the EASM-TA relationship. When the EASM-TA has a significantly positive (insignificantly and slightly negative) relationship, the IPO is in its positive (negative) phase. Such covariation is not strictly consistent before the 1920s due to the poor quality and sparsity of observations. In this study, we assume the IPO as the potential factor that modulates the EASM-TA relationship. As selected in Fig. 1b, the highly correlated period of 1978–1998 corresponds to the pIPO period, while the insignificantly correlated period of 1951–1971 corresponds to the nIPO period. We use these two periods to investigate the physical processes of the IPO in modulating the interdecadal variation of the EASM-TA relationship.

The interdecadal IPO modulates the interannual variation in the EASM-TA relationship

During the two periods, the strength of interannual variability of the EASM reacts quite differently to the TA SST. In the pIPO period, the interannual strength of the EASM strongly responds to the change of the TA SST (Fig. 2a). The EASM becomes stronger (weaker) when the TA gets warmer (cooler). The two variables exhibit a significantly positive correlation coefficient of 0.49, above the 95% confidence level. In contrast, The EASM and TA SST show an insignificantly negative relationship in the nIPO period, with the correlation coefficient of -0.27 (Fig. 2b), far below the 80% confidence level. This result implies that TA SST has little impact on the interannual EASM during the nIPO period. Given that the anomalous TA SST can change the Walker circulation^{20,22,31}, we compare the interannual response of the JJA tropical Pacific SST to the interannual TA SST variation in different IPO periods (Fig. 2c, d). In the pIPO period, there is a significant cooling pattern in the CTP, as pointed out in many previous papers^{20,22,30–34}, which means that CTP SST cooling is closely related to the interannual warming of TA SST during the pIPO period. However, an insignificant warming pattern in the CTP appears in the nIPO period. This indicates that interannual TA SST warming (cooling) is unable to result in interannual CTP SST cooling (warming) during the nIPO period. The TA SST-induced SST changes in the CTP will subsequently change the atmospheric circulation over the western north Pacific to influence the strength of the EASM.

Here, we show the response of atmospheric circulation over the western north Pacific to the TA SST in different IPO periods by regressing JJA SLP and 850-hPa wind anomalies against the JJA TA SST index (Fig. 3). In Fig. 3a, the diabatic cooling of CTP SST resulting from TA SST warming can excite WNPAC with a significantly high SLP center located around 20°N in the pIPO

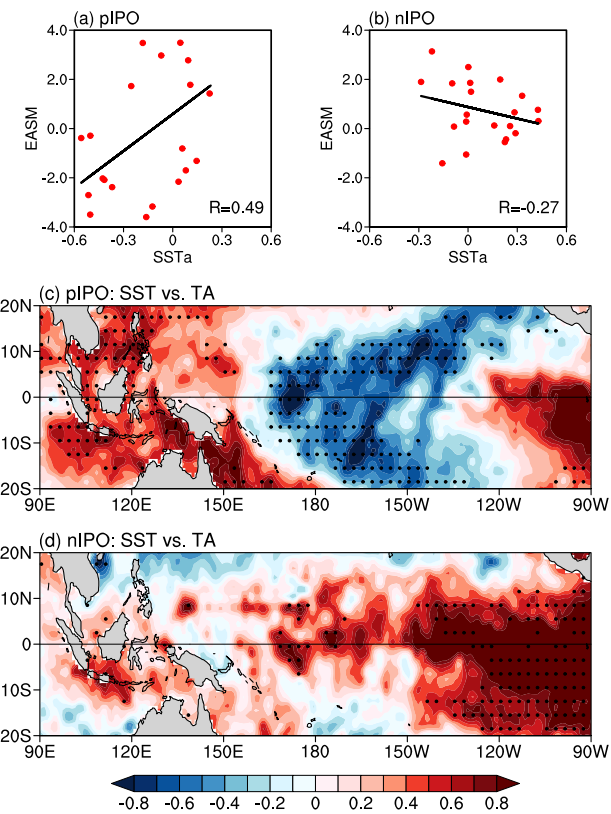


Fig. 2 The contrast EASM-TA relationships and comparison of CTP SST response to TA SST variation in different IPO periods. **a** Scatterplot between the EASM and SST anomaly in the TA during the positive phase of the IPO. **b** Same as (a), but during the negative phase of the IPO. **c** Regression map of JJA SST anomalies ($^{\circ}\text{C}$) onto JJA TA SST index during the positive phase of the IPO. **d** Same as (c), but during the negative phase of the IPO. The dotted area in **c, d** indicates that the value is significant at the 95% confidence level using Student's *t*-test.

period, accompanied by evident easterly winds extending from the western tropical Pacific to the Bay of Bengal. The southeasterly winds over tropical–subtropical East Asia caused by WNPAC can enhance the EASM and transport moist air from the tropics to eastern China. Thus, the JJA EASM and TA SST are highly correlated during the pIPO period (Fig. 2a). However, these atmospheric circulation changes cannot occur in the nIPO period. Compared with the pIPO period, there are only weak northeasterly winds over eastern China, which may hinder the enhancement of the EASM, and the significantly high SLP center of WNPAC is absent due to the absence of TA SST-induced CTP SST cooling (Fig. 3b). Hence, the interannual EASM–TA relationship is insignificant during the nIPO period (Fig. 2b). The different atmospheric circulation response in the two periods leads to the changing strength of the linkage between the EASM and TA SST. These different responses of atmospheric circulation over the western North Pacific to TA SST are strictly under the thermodynamic framework of Matsuno–Gill Response^{47,48}. Why is the strength of Matsuno–Gill response to the CTP SST different during different IPO phases?

To answer this question, we plot an interdecadal IPO pattern through the correlation map between the global SST and IPO index (Fig. 4a). Many previous papers investigating the role of the IPO in the EASM mainly focused on the changes in the subtropical high associated with the IPO³⁸, but paid less attention on its tropical part. Apart from the classical horseshoe-shaped warming (cooling) pattern in the northern hemisphere, the central to eastern tropical Pacific also has a significant warming (cooling)

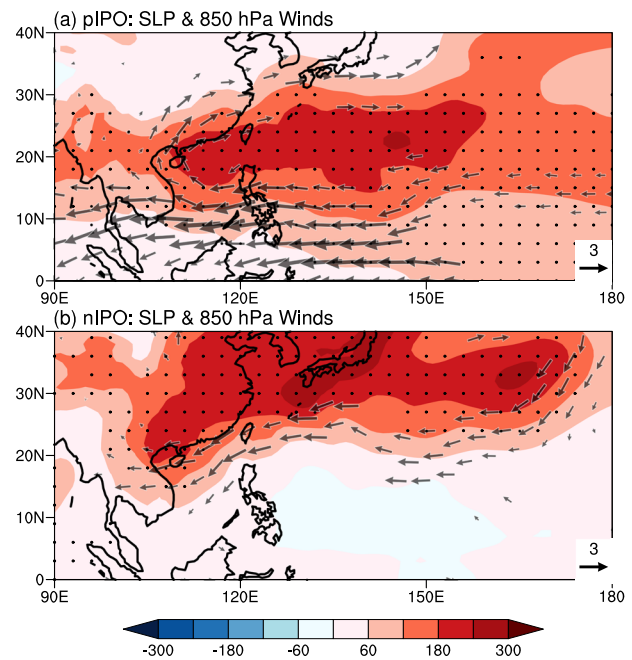


Fig. 3 The comparison of JJA atmospheric circulation response to TA SST variation in different IPO periods. The JJA SLP (shaded, units: Pa) and 850-hPa wind (vectors, units: m s^{-1}) regressed onto JJA TA SST index during **a** the positive phase and **b** the negative phase of the IPO. The dots indicate that the value is significant at the 95% confidence level using Student's *t*-test. The 850-hPa wind is shown when the meridional or zonal component is significant at the 95% confidence level using Student's *t*-test.

pattern during the pIPO (nIPO) phase. In the pIPO (nIPO) period, when the CTP is warmer (cooler), there is more (less) convective available potential energy over the central-eastern tropical Pacific, implying more (less) active activities of the atmosphere and stronger (weaker) background atmospheric convection (Supplementary Fig. 3). Thus, such CTP warming (cooling) will intensify (weaken) the convection and resultant precipitation over the CTP (Supplementary Fig. 4). These IPO-induced mean state changes will further modulate the EASM–TA relationship. On interannual timescales, TA SST warming (cooling) will lead to an anomalous descending (ascending) motion over the CTP, producing a diabatic cooling (heating) to excite the WNPAC (WNPC)^{20,22,31}.

Considering the role of the IPO on interdecadal timescales, the TA-induced descending motion from warmer TA over CTP will produce a greater diabatic cooling due to the background stronger convection in the pIPO period^{38,49}. It is shown that, in the pIPO period, when the background convection is strong, the TA SST warming could reduce the precipitation through the descending motion over the CTP (Supplementary Fig. 5a). The reduced precipitation could further suppress the heat release of the water vapor condensation. However, the TA warming could not significantly reduce the precipitation during the nIPO period since the background convection over the CTP is relatively weak (Supplementary Fig. 5b). Therefore, there is greater diabatic cooling during the pIPO period than that during the nIPO period. Such greater diabatic cooling will excite a stronger WNPAC through the Matsuno–Gill response to produce a stronger influence of TA SST on the EASM through the CTP. Therefore, there is a strong interannual linkage between the TA and EASM in the pIPO period. As shown in Fig. 4c, in the nIPO period, there is no significant TA-induced descending motions over the CTP since the nIPO-related CTP cooling background will weaken the Matsuno–Gill response. Therefore, the interannual influence of TA SST on the EASM is weakened, and the EASM–TA interannual

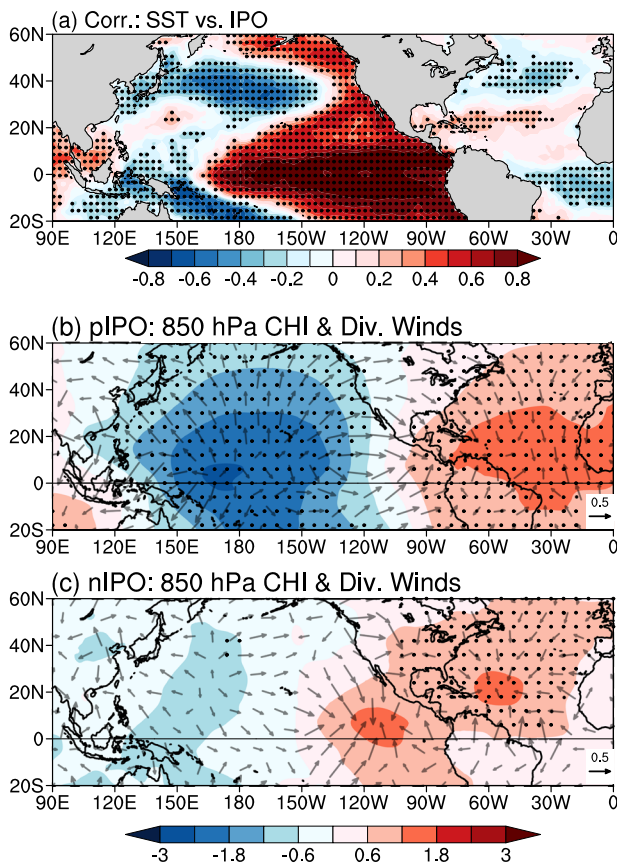


Fig. 4 The IPO climatological mean state controls the JJA large-scale atmospheric response to TA SST. a Correlation map between the SST and IPO index. **b** The JJA velocity potential (shaded) and the divergent wind (vectors) at 850 hPa regressed onto the JJA TA SST index during the positive phase of the IPO. **c** Same (b), but for the negative phase of the IPO. The dots indicate a value that is significant at the 95% confidence level using Student's *t*-test.

relationship is insignificant in the nIPO period. These processes can be confirmed from the regression map of 850-hPa velocity potential and divergent wind anomalies against the TA index (Fig. 4b, c). The negative center of 850-hPa velocity potential and accompanied divergent winds over the CTP are significantly stronger in the pIPO period than those in the nIPO period. Besides, the TA-induced Walker circulation is much stronger in the pIPO period than in the nIPO period (Supplementary Fig. 6). The above analyses show that the IPO-related mean state changes in the CTP on decadal timescales will intensify or weaken the Matsuno–Gill response of the diabatic heating associated with the TA-induced CTP SST change on interannual timescales to modulate the EASM–TA relationship on interdecadal timescales and lead to the interdecadal variation in the interannual EASM–TA relationship.

DISCUSSION

We have found that there is evident interdecadal variation in the interannual EASM–TA relationship, and this interdecadal variation is modulated by the IPO. The EASM–TA relationship is insignificant and even slightly negative in the nIPO period of 1951–1971 but turns into significantly positive in the pIPO period of 1978–1998. The pIPO (nIPO)-related warm (cold) CTP SST can enhance (weaken) the convection and precipitation over the CTP. The pIPO favors a stronger atmospheric response because the background atmospheric convection is stronger over the warm SST condition in the CTP. The atmosphere is more active under the

stronger convection background over the CTP during the pIPO period; thus, the TA-induced anomalous convection is much more obvious during the pIPO period than that during the nIPO period. Such mean state changes associated with the IPO will modulate the EASM–TA relationship on interannual timescales. The pIPO-related warm CTP SST can intensify the Matsuno–Gill response of the TA-induced CTP SST cooling, as the TA-induced anomalous descending motion over the CTP has a stronger diabatic cooling effect. However, the nIPO-related CTP SST cooling can weaken the Matsuno–Gill response of the TA-induced CTP SST cooling. A stronger Matsuno–Gill response will excite the WNPAC to enhance the EASM, demonstrating a strong EASM–TA relationship in the pIPO period. By contrast, the TA-induced WNPAC is absent in the nIPO period due to the weak Matsuno–Gill response, leading to a weak response of the EASM to TA SST. Thus, as a result of the different strengths of Matsuno–Gill response, the EASM–TA relationship is strong during the pIPO period but weak during the nIPO period. In the above research, one pIPO period and one nIPO period are used. So, we have also compared the EASM–TA relationship in other IPO periods to see the sharp contrast of the EASM–TA relationship (Supplementary Fig. 7). From 1902 to 1922, when the IPO turned slightly negative, the EASM–TA relationship is weak and insignificant. But it turned into strong and significant during the pIPO period (1926–1946). The result highlights the interdecadal variability in the interannual EASM–TA SST relationship and the possible influence of the IPO. The modulation of TA SST anomalies on summer climate in the western North Pacific could also be modulated by some other climatic factors. For example, the weakened Atlantic thermohaline circulation in the 1960s may change the mean state of the North Atlantic to strengthen the impact of the TA SST anomalies on the western North Pacific⁵⁰. The relative roles and contributions of these climatic factors need further detailed research. Our results highlight the importance of the IPO in modulating the interannual EASM–TA relationship, and the phase of the IPO should be taken into consideration while performing seasonal forecasts of the EASM.

METHODS

Data

The NOAA-CIRES-DOE 20th Century Reanalysis V3 dataset (20CRv3) is used to provide monthly atmospheric variables, including sea level pressure (SLP), winds, and convective available potential energy, with a horizontal resolution of $1^\circ \times 1^\circ$ ⁵¹, covering the time period of 1836/01 to 2015/12. The 20CRv3 dataset has been widely used to investigate the general atmospheric circulation and associated long-term changes^{52–54}. We also use monthly SST from the Met Office Hadley Center (HadISST1) at a horizontal resolution of $1^\circ \times 1^\circ$ ⁵⁵. All variables are focused on the period from 1900 to 2015, and the global warming signal is removed from all variables by using linear detrending.

EASM index

The EASM index is defined as the JJA mean difference between 850-hPa zonal wind averaged over $22.5^\circ\text{--}32.5^\circ\text{N}$, $110^\circ\text{--}140^\circ\text{E}$ and $5^\circ\text{--}15^\circ\text{N}$, $90^\circ\text{--}130^\circ\text{E}$ ^{36,56}. Here, we use the opposite sign of the EASM index, intuitively indicating a strong (weak) EASM year with a positive (negative) EASM index.

ENSO index

The December–January–February (DJF) Nino-3.4 index in the preceding year is used as the proxy of the ENSO index, which is defined by the area-averaged SST anomaly over $5^\circ\text{S}\text{--}5^\circ\text{N}$, $120^\circ\text{--}170^\circ\text{W}$.

As ENSO events have an overwhelming influence on the EASM from its developing to decay phases^{1,8,10,11,15,18,38}, we remove the ENSO signal by using the linear regression^{30,57}.

$$y = ax + b, \quad (1)$$

where, y represents the variable, and x is the DJF(-1) ENSO index. In the linear regression analysis, ax represents the ENSO-related y and b represents the part independent of the ENSO signal.

IPO index

The IPO index is defined as the leading mode extracted from the empirical orthogonal function (EOF) analysis on the 9-year low pass filtered JJA SST over the Pacific Ocean^{42,58,59}.

Statistical significance test

In this study, correlation and regression are used to measure the relationship between two variables, and the significance test is based on the effective sample numbers N_{eff} by the following formula:^{60,61}

$$\frac{1}{N_{\text{eff}}} \approx \frac{1}{N} + \frac{2}{N} \sum_{j=1}^{N-2} \frac{N-j}{N} \rho_{XX}(j) \rho_{YY}(j), \quad (2)$$

here, N is the sample size, ρ_{XX} and ρ_{YY} represent the autocorrelations of the time series X and Y at lag j , individually.

DATA AVAILABILITY

The 20CRv3 dataset was obtained from https://psl.noaa.gov/data/gridded/data.20thC_ReanV3.html. The HadISST1 dataset was obtained from <https://www.metoffice.gov.uk/hadobs/hadisst/>.

CODE AVAILABILITY

Codes used in this manuscript are available upon reasonable requests from the corresponding author.

Received: 19 June 2023; Accepted: 11 October 2023;

Published online: 24 October 2023

13. Li, S., Lu, J., Huang, G. & Hu, K. Tropical Indian Ocean basin warming and East Asian summer monsoon: a multiple AGCM study. *J. Clim.* **21**, 6080–6088 (2008).
14. Du, Y., Xie, S.-P., Huang, G. & Hu, K. Role of air-sea interaction in the long persistence of El Niño-Induced North Indian ocean warming. *J. Clim.* **22**, 2023–2038 (2009).
15. Xie, S.-P. et al. Indian Ocean capacitor effect on Indo-Western Pacific climate during the summer following El Niño. *J. Clim.* **22**, 730–747 (2009).
16. Gong, D. Y. et al. Spring Arctic Oscillation-East Asian summer monsoon connection through circulation changes over the western North Pacific. *Clim. Dyn.* **37**, 2199–2216 (2011).
17. Sung, M.-K. et al. A possible impact of the North Atlantic Oscillation on the East Asian summer monsoon precipitation. *Geophys. Res. Lett.* **33**, L21713 (2006).
18. Wu, Z., Wang, B., Li, J. & Jin, F.-F. An empirical seasonal prediction model of the East Asian summer monsoon using ENSO and NAO. *J. Geophys. Res.* **114**, D18120 (2009).
19. Sun, J. & Wang, H. Changes of the connection between the summer North Atlantic Oscillation and the East Asian summer rainfall. *J. Geophys. Res.* **117**, D08110 (2012).
20. Jin, D. & Huo, L. Influence of tropical Atlantic sea surface temperature anomalies on the East Asian summer monsoon. *Q. J. R. Meteorol. Soc.* **144**, 1490–1500 (2018).
21. Choi, Y. W. & Ahn, J. B. Possible mechanisms for the coupling between late spring sea surface temperature anomalies over tropical Atlantic and East Asian summer monsoon. *Clim. Dyn.* **53**, 6995–7009 (2019).
22. Ren, H., Zuo, J. & Li, W. The impact of tropical Atlantic SST variability on the tropical atmosphere during Boreal summer. *J. Clim.* **34**, 6705–6723 (2021).
23. Zebiak, S. E. Air-sea interaction in the equatorial Atlantic region. *J. Clim.* **6**, 1567–1586 (1993).
24. Enfield, D. B. & Mayer, D. A. Tropical Atlantic sea surface temperature variability and its relation to El Niño-Southern Oscillation. *J. Geophys. Res.* **102**, 929–945 (1997).
25. Liu, Z., Zhang, Q. & Wu, L. Remote impact on tropical Atlantic climate variability: statistical assessment and dynamic assessment. *J. Clim.* **17**, 1529–1549 (2004).
26. Huang, B. & Shukla, J. Ocean-atmosphere interactions in the tropical and subtropical Atlantic Ocean. *J. Clim.* **18**, 1652–1672 (2005).
27. Ding, H., Keenlyside, N. S. & Latif, M. Impact of the equatorial Atlantic on the El Niño Southern Oscillation. *Clim. Dyn.* **38**, 1965–1972 (2012).
28. Vitthal, H., Villarini, G. & Zhang, W. Early prediction of the Indian summer monsoon rainfall by the Atlantic Meridional Mode. *Clim. Dyn.* **54**, 2337–2346 (2020).
29. Fan, L., Shin, S. I., Liu, Q. Y. & Liu, Z. Y. Relative importance of tropical SST anomalies in forcing east Asian summer monsoon circulation. *Geophys. Res. Lett.* **40**, 2471–2477 (2013).
30. Ham, Y.-G., Kug, J.-S., Park, J.-Y. & Jin, F.-F. Sea surface temperature in the north tropical Atlantic as a trigger for El Niño/Southern Oscillation events. *Nat. Geosci.* **6**, 112–116 (2013).
31. Hong, C., Chang, T. & Hsu, H. Enhanced relationship between the tropical Atlantic SST and the summertime western North Pacific subtropical high after the early 1980s. *J. Geophys. Res.* **119**, 3715–3722 (2014).
32. Chang, T. C., Hsu, H.-H. & Hong, C.-C. Enhanced influences of tropical Atlantic SST on WNP-NIO atmosphere-ocean coupling since the early 1980s. *J. Clim.* **29**, 6509–6525 (2016).
33. Ruprich-Robert, Y. et al. Assessing the Climate Impacts of the Observed Atlantic Multidecadal Variability Using the GFDL CM2.1 and NCAR CESM1 Global Coupled Models. *J. Clim.* **30**, 2785–2810 (2017).
34. Meehl, G. A. et al. Atlantic and Pacific tropics connected by mutually interactive decadal-timescale processes. *Nat. Geosci.* **14**, 36–42 (2021).
35. Zuo, J., Li, W., Sun, C. & Ren, H. Remote forcing of the northern tropical Atlantic SST anomalies on the western North Pacific anomalous anticyclone. *Clim. Dyn.* **52**, 2837–2853 (2018).
36. Wang, B. et al. How to measure the strength of the east Asian summer monsoon. *J. Clim.* **21**, 4449–4463 (2008).
37. Xie, S.-P. et al. Decadal shift in El Niño influences on Indo-western Pacific and East Asian climate in the 1970s. *J. Clim.* **23**, 3352–3368 (2010).
38. Song, F. & Zhou, T. The dominant role of internal variability in modulating the decadal variation of the East Asian summer monsoon-ENSO relationship during the 20th century. *J. Clim.* **28**, 7093–7107 (2015).
39. Chen, S., Chen, W., Wu, R. & Song, L. Impacts of the Atlantic multidecadal oscillation on the relationship of the spring arctic oscillation and the following East Asian summer monsoon. *J. Clim.* **33**, 6651–6672 (2020).
40. Liu, K., Zhou, L., Wang, Z., Liu, Y. & Yin, X. Interdecadal Strengthening in the independent relationship between the East Asian Summer Monsoon and the Indian Ocean Basin Mode around the Early 1990s. *J. Clim.* **34**, 6759–6776 (2021).
41. Mantua, N. J., Hare, S. R., Zhang, Y., Wallace, J. M. & Francis, R. C. A Pacific interdecadal climate oscillation with impacts on salmon production. *Bull. Am. Meteorol. Soc.* **78**, 1069–1079 (1997).

42. Folland, C. K., Parker, D. E., Colman, A., & Washington, R. Large scale modes of ocean surface temperature since the late nineteenth century, in *Beyond El Niño: Decadal and Interdecadal Climate Variability*, vol. 4, (ed Navarra, A.) 73–102 (Springer, 1999).
43. Dong, B. & Dai, A. The influence of the Interdecadal Pacific Oscillation on temperature and precipitation over the globe. *Clim. Dyn.* **45**, 2667–2681 (2015).
44. Zhang, Y., Xie, S.-P., Kosaka, Y. & Yang, J.-C. Pacific decadal oscillation: tropical Pacific forcing versus internal variability. *J. Clim.* **31**, 8265–8279 (2018).
45. Mestas-Nunez, A. & Enfield, D. B. Rotated global modes of non-ENSO sea surface temperature variability. *J. Clim.* **12**, 2734–2746 (1999).
46. Kerr, R. A. A North Atlantic climate pacemaker for the centuries. *Science* **288**, 1984–1986 (2000).
47. Matsuno, T. Quasi-geostrophic motions in the equatorial area. *J. Meteorol. Soc. Jpn.* **44**, 25–43 (1966).
48. Gill, A. E. Some simple solutions for heat-induced tropical circulation. *Q. J. R. Meteorol. Soc.* **106**, 447–462 (1980).
49. Huang, Y., Wu, B., Li, T., Zhou, T. & Liu, B. Interdecadal Indian Ocean basin mode driven by Interdecadal Pacific Oscillation: a season-dependent growth mechanism. *J. Clim.* **32**, 2057–2073 (2019).
50. Chen, W., Lee, J.-Y., Lu, R., Dong, B. & Ha, K.-J. Intensified impact of tropical Atlantic SST on the western North Pacific summer climate under a weakened Atlantic thermohaline circulation. *Clim. Dyn.* **45**, 2033–2046 (2014).
51. Slivinski, L. C. et al. Towards a more reliable historical reanalysis: Improvements for version 3 of the Twentieth Century Reanalysis system. *Q. J. R. Meteorol. Soc.* **145**, 2876–2908 (2019).
52. Slivinski, L. C. et al. An evaluation of the performance of the twentieth century reanalysis version 3. *J. Clim.* **34**, 1417–1438 (2021).
53. Bracegirdle, T. J. Early-to-late winter 20th century North Atlantic multidecadal atmospheric variability in observations, CMIP5 and CMIP6. *Geophys. Res. Lett.* **49**, e2022GL098212 (2022).
54. Zhang, Y. et al. Atmospheric forcing of the Pacific Meridional Mode: tropical Pacific-driven versus internal variability. *Geophys. Res. Lett.* **49**, e2022GL098148 (2022).
55. Rayner, N. A. et al. Global analyses of sea surface temperature, sea ice, and night marine air temperature since the late nineteenth century. *J. Geophys. Res.* **108**, 4407 (2003).
56. Wang, B. & Fan, Z. Choice of South Asian summer monsoon indices. *Bull. Am. Meteorol. Soc.* **80**, 629–638 (1999).
57. Chen, S., Wu, R. & Chen, W. Modulation of spring northern tropical Atlantic sea surface temperature on the El Niño–Southern Oscillation—east Asian summer monsoon connection. *Int. J. Climatol.* **38**, 5020–5029 (2018).
58. Folland, C. K., Renwick, J. A., Salinger, M. J. & Mullan, A. B. Relative influences of the Interdecadal Pacific Oscillation and ENSO on the South Pacific convergence zone. *Geophys. Res. Lett.* **29**, 1643 (2002).
59. Power, S., Casey, T., Folland, C., Colman, A. & Mehta, V. Inter-decadal modulation of the impact of ENSO on Australia. *Clim. Dyn.* **15**, 319–324 (1999).
60. Pyper, B. J. & Peterman, R. M. Comparison of methods to account for auto-correlation in correlation analyses of fish data. *Can. J. Fish. Aquat. Sci.* **55**, 2127–2140 (1998).
61. Li, J., Sun, C. & Jin, F. F. NAO implicated as a predictor of Northern Hemisphere mean temperature multidecadal variability. *Geophys. Res. Lett.* **40**, 5497–5502 (2013).

ACKNOWLEDGEMENTS

The research was supported by the National Natural Science Foundation of China (42376022), the Hainan Provincial Joint Project of Sanya Yazhou Bay Science and Technology City (2021JYLH0056), the National Natural Science Foundation of China (41925025, 92058203, and 41975089) and China's National Key Research and Development Projects (2018YFA0605704). Y.Z. was supported by Laoshan Laboratory (No. LSKJ202202602), the Fundamental Research Funds for the Central Universities (202213050), and the China Postdoctoral Science Foundation (2021M703034).

AUTHOR CONTRIBUTIONS

H.W. and Z.L. designed the study, prepared all the figures, and wrote the paper. All the authors discussed the study results and reviewed the paper.

COMPETING INTERESTS

The authors declare no competing interests.

ADDITIONAL INFORMATION

Supplementary information The online version contains supplementary material available at <https://doi.org/10.1038/s41612-023-00497-x>.

Correspondence and requests for materials should be addressed to Ziguang Li.

Reprints and permission information is available at <http://www.nature.com/reprints>

Publisher's note Springer Nature remains neutral with regard to jurisdictional claims in published maps and institutional affiliations.



Open Access This article is licensed under a Creative Commons Attribution 4.0 International License, which permits use, sharing, adaptation, distribution and reproduction in any medium or format, as long as you give appropriate credit to the original author(s) and the source, provide a link to the Creative Commons license, and indicate if changes were made. The images or other third party material in this article are included in the article's Creative Commons license, unless indicated otherwise in a credit line to the material. If material is not included in the article's Creative Commons license and your intended use is not permitted by statutory regulation or exceeds the permitted use, you will need to obtain permission directly from the copyright holder. To view a copy of this license, visit <http://creativecommons.org/licenses/by/4.0/>.

© The Author(s) 2023